Capillary Filling in Nanochannels – Modeling, Fabrication and Experiments

Author

Phan, Vinh Nguyen, Joseph, Pierre, Djeghlaf, Lyes, Allouch, Alaa El Dine, Bourrier, David, Abgrall, Patrick, Gue, Anne-Marie, Yang, Chun, Nguyen, Nam-Trung

Published

2011

Journal Title

Heat Transfer Engineering

DOI

10.1080/01457632.2010.509756

Capillary Filling in Nanochannels – Modeling, Fabrication, and Experiments

Vinh Nguyen Phan,[1] Pierre Joseph,[2] Lyes Djeghlaf,[2] Alaa El Dine Allouch,[2] David Bourrier,[2] Patrick Abgrall,[1] Anne-Marie Gué,[2] Chun Yang,[1] and Nam-Trung Nguyen[1*]

[1] School of Mechanical and Aerospace Engineering, Nanyang Technological University, Singapore

[2] LAAS-CNRS and Université de Toulouse, Toulouse, France

ABSTRACT

While capillary filling in channels of micrometers scale is experimentally verified to obey Washburn's law well, the speed of capillary filling in nanochannels is noticeable lower than described by Washburn's formula. This article reports the theoretical and experimental results on capillary filling in open-end and closed-end nanochannels. Nanochannels of 45 nm and 80 nm depth, 10 μm width, were etched in silicon and bonded to a glass cover. Experiments on filling of non-electrolytic liquid in silicon nanochannels were carried out. The filling processes were observed and recorded. To estimate the influence of electrokinetics, a mathematical model to calculate the electroviscous effect was established. This model shows that contribution of electroviscous effect in the reduction of filling speed is small. This result also agrees well with previous theoretical work on the electroviscous effect. That means besides the electroviscous effect, there are other phenomena that contribute to the reduction of capillary filling speed in a nanochannel, such as air bubbles formation. Experimental investigation of capillary filling in open-end and closed-end nanochannels with different lengths was performed. The filling processes of ethanol and isopropanol and the behavior of the trapped air were recorded and evaluated. Analytical models based on the continuum assumption were used to evaluate the experimental data. We observed that the filling process consists of two stages. At the initial stage, experimental data agree well with the theoretical model, but with a higher apparent viscosity. In the final stage, condensation of the liquid phase and dissolution of the gas phase lead to total filling of the nanochannel. The observed phenomena are important for understanding the behavior of multiphase systems in nanochannels.

[*] Address correspondence to Professor Nam-Trung Nguyen, School of Mechanical and Aerospace Engineering, Nanyang Technological University, 50 Nanyang Avenue 639798, Singapore. E-mail: mntnguyen@ntu.edu.sg

INTRODUCTION

The increasing use of semiconductor devices and the increasing spatial density of these devices lead to the demand for new technologies for heat exchangers [1]. As air-cooling technology may soon become insufficient, liquid cooling promises to replace air-cooling technology in the near future [2]. The higher heat transfer rate is based on the fact that heat conductivity of liquid is generally higher than that of air. For instance, the heat conductivity of water of 0.58 W/m-K is more than 20 times of that of air (0.024 W/m-K). Thermal properties of liquid flow in microchannels and millichannels have been studied intensively in the past [3]. Weisberg et al. [4] numerically investigated a heat exchanger using microchannels. The authors also suggested a formulation to design such a heat exchanger. Peng et al. performed a series of works [5-8] on liquid flow and heat transfer in microchannels. Similar investigations of fluid flow and heat transfer in microchannels and their applications were discussed by other authors [9-14].

As the characteristic size of the channel gets smaller, the ratio between surface area and volume increases. Therefore, microscale phenomena are more favorable for heat transfer [15]. However, studies on heat transfer in nanochannels with characteristic dimensions ranging from several to hundreds of nanometers are still at an early stage. One of the difficulties in investigation of heat transfer in at the nanoscale is that the transport phenomena of fluid flow in nanostructure have not been fully understood.

In recent years, advances in micro/nanotechnologies allowed the fabrication of structures at nanoscale [16-21]. Various techniques and devices for transport, handling, and manipulating fluid in micro-/nanoscale were developed [22-24]. These technological advances allow more sophisticated investigation of transport phenomena in nanoscale. Many experiments on capillary filling in nanochannels have been carried out in recent years [25-30]. The experimental results revealed that capillary filling in nanochannel qualitatively follows Washburn's equation. However, the filling speed observed experimentally is usually lower than expected by the classic Washburn's formula, which is equivalent to an increase in apparent viscosity.

Several efforts were reported to explain the variation between experimental and theoretical results of capillary filling in nanochannels. Van Honschoten et al. [31] suggested a model of elastocapillary filling in deformable channels. The deformation of nanochannels due to high negative pressure across the meniscus may cause variation in apparent viscosity. Because of the high surface-to-volume ratio of the nanochannels, it is believed that surface effects such as electroviscous effect contribute to the increase in apparent viscosity [32-35]. Han et al. [26] investigated the filling kinetics of different liquids in nanochannels with rectangular cross section. Trapping of air bubbles during the filling processes was observed.

The formation of air bubbles depends on the interaction between gas and liquid in nanoscale. However, most of the knowledge gained in the past was based on macroscopic investigation of porous materials. For instance, Shaw reported

experimental results of the evaporation process in porous materials [36]. This work set the foundation for subsequent research on modeling of drying processes in porous materials. Prat used the invasion percolation theory to model the drying process in porous material [37]. Yiotis et al. presented a theoretical model for the drying process in porous materials [38]. The results showed that the formation of a liquid film accelerates the drying process.

In this article, we report theoretical and experimental results on capillary filling in open-end and closed-end nanochannels. Capillary filling experiment in the open-end nanochannel were performed with non-electrolytic liquids (ethanol and isopropanol) to minimize possible electroviscous effects. A simple mathematical model to evaluate the contribution of electroviscous effect in the increase of apparent viscosity is also introduced. The results from the theoretical model are then compared to the experimental value above to estimate the general significance of electroviscous effect in the overall increase of apparent viscosity. Closed-end nanochannels offer an ideal platform for studying multiphase-related phenomena at the nanoscale, such as condensation. In our work, quantitative measurements of filling lengths versus time were obtained for isopropanol and ethanol. We also investigated the behavior of trapped air during the filling process. Under the high Laplace pressure, condensation of the liquid phase followed by dissolution of the gas phase are the main phenomena observed in the nanoscale confinement.

THEORY

Capillary filling in open-end and closed-end planar nanochannels with a height of *h*, a width of w, and an aspect ratio of $w/h >> 1$ is considered. The driving force depends on the surface tension of the fluid and the contact angle between the fluid and the channel wall

$$F_s = 2\sigma w \cos\theta \qquad (1)$$

where F_s is the capillary force at the contact line caused by surface tension σ, and θ is the contact angle between the fluid and the wall surface. In this investigation, the variation of surface energy due to accumulation of charged particles near the meniscus, as described in the Gibbs-Duhem equation, is ignored. It was reported in the literature that the liquid slip at the solid-liquid interface [39] and the interaction with electrokinetic effects [40] may lead to modification of effective contact angle. However, in capillary filling of nanochannels the shear stress and streaming voltage diminish quickly. Under such condition the change in effective contact angle is negligible. The velocity profile in capillary filling flow is considered the same as in pressure-driven flow. Due to low Reynolds number, the flow resistance caused by an entrance effect as discussed in recent investigation [41-44] is ignored. In the case of a planar nanochannel, the velocity profile has a parabolic form [45]. The viscous force is then given by

$$F_{\mathrm{v}} = \left(\mu \frac{du}{dy}\bigg|_{y=\frac{h}{2}} - \mu \frac{du}{dy}\bigg|_{y=-\frac{h}{2}} \right) wx = -\frac{12\mu\bar{u}}{h} wx \tag{2}$$

where F_{v} is the viscosity force acting on the fluid, x is the filling length, $\bar{u} = \mathrm{d}x/\mathrm{d}t$ is the filling speed, and μ is the dynamic viscosity of the fluid. The filling process is considered to begin at the entrance of the channel; hence the initial condition $x = 0$ at $t = 0$ is applied to both closed-end and open-end nanochannels.

Capillary Filling in Open-End Nanochannels

Figure 1 a shows the model of capillary filling process in an open-end nanochannel, with consideration of electroviscous effect. Without any lost of generality, the wall of the channel is assumed to be positively charged, through the selective absorption of cations. The shaded areas in Figure 1 a represent the electrical double layer (EDL). The streaming voltage caused by the accumulation of anion at the meniscus generated a conductive current, as well as the electric force against the filling movement. The reduction of filling speed represents the increase in apparent viscosity [46].

In a nanochannel, the electric potential distribution and the charge density distribution is governed by the Poisson-Boltzmann (PB) equation [47, 48]:

$$\nabla^2 \Psi = -\frac{\rho_{\mathrm{q}}}{\varepsilon\varepsilon_0} = -\frac{e}{\varepsilon\varepsilon_0} \sum_i z_i n_i^0 \exp\left(-\frac{z_i e \Psi}{kT} \right) \tag{3}$$

where Ψ is the electrostatic potential, ρ_{q} is the charge density, $e = 1.6021 \times 10^{-19}\,\mathrm{C}$ is the elementary charge, ε is the relative permittivity of the fluid, $\varepsilon_0 = 8.854 \times 10^{-12}\,\mathrm{CV^{-1}m^{-1}}$ is the permittivity of vacuum, z_i is the charge number of ionic species i, n_i^0 is the bulk concentration of ionic species i, $k = 1.381 \times 10^{-23}\,\mathrm{JK^{-1}}$ is Boltzmann's constant, and T is the temperature. Applying Debye-Hückel approximation of low potential for binary electrolyte (i.e. $z_1 = z_2 = z$), the potential distribution is given by [48]

$$\Psi(y) = \zeta \frac{\cosh(-\kappa y)}{\cosh(\kappa h/2)} \tag{4}$$

and the charge density distribution is given by

$$\rho_q = -\varepsilon\varepsilon_0 \frac{d^2\Psi}{dy^2} = -\varepsilon\varepsilon_0 \zeta \kappa^2 \frac{\cosh(\kappa y)}{\cosh(\kappa h/2)} \tag{5}$$

where κ is the Debye parameter and $\kappa^2 = \dfrac{2e^2 z^2 n^0}{\varepsilon\varepsilon_0 kT}$ (n^0 is the bulk concentration of the solute). The Debye-Hückel approximation is only valid for ζ potential below 26 mV [49]. Studies in reported literature describe the solution of the PB equations in

other conditions [32, 34, 35, 50-59]. These results can be applied in our model by substituting the Eq. (4) accordingly. In such cases, the final equations should be more difficult to be solved.

Considering the redistribution of charge density, the average conductivity of the monovalent electrolyte, such as NaCl solution, in nanochannels is given by

$$\bar{\lambda} = n^0 \frac{\Lambda_\mathrm{m}}{N_\mathrm{A}} \left(1 + \frac{\zeta e}{kT} \frac{\nu_- - \nu_+}{\nu_+ + \nu_-} \frac{2 \tanh\left(\frac{\kappa h}{2} \right)}{\kappa h} \right) \tag{6}$$

where ν_i is the electrical mobility of ionic species i and $\Lambda_\mathrm{m} = \sum_i e N_\mathrm{A} \nu_i$ is the molar conductivity of a monovalent electrolyte.

The charge balance is considered with streaming current, conductive current and accumulated charge. The charge balance is then expressed by

$$-\frac{q_\mathrm{a} \bar{\lambda}}{\varepsilon \varepsilon_0} + \int_{-\frac{h}{2}}^{\frac{h}{2}} u \rho_\mathrm{q} w \mathrm{d}y = \frac{d}{dt} q_\mathrm{a} \tag{7}$$

The electric charge accumulated at the front of the fluid column produces an electric field, namely the streaming potential field. Such an electric field in turn causes electrostatic force acting on the entire liquid column. Assuming a constant electric field along the channel, the electric force is

$$F_\mathrm{e} = -x \int_{A_\mathrm{c}} \frac{U_\mathrm{s}}{x} \rho_\mathrm{q} \mathrm{d}A_\mathrm{c} = -xw \int_{-\frac{h}{2}}^{\frac{h}{2}} \frac{U_\mathrm{s}}{x} \rho_\mathrm{q} \mathrm{d}y \tag{8}$$

where U_S is the streaming potential, which is the electric potential difference between the meniscus and the entrance of the channel.

The force balance on the moving liquid column is expressed according to Newton's second law [60]

$$F_\mathrm{s} + F_\mathrm{v} + F_\mathrm{e} = \frac{\mathrm{d}}{\mathrm{d}t} \left(\rho_\mathrm{m} whx \bar{u} \right) \tag{9}$$

where F_e is the electric force and ρ_m is the mass density of the fluid.

From the force balance and the charge balance, the equation system for the capillary filling effect in a nanochannel is expressed as

$$\begin{cases} 2\sigma w\cos\theta-\dfrac{12\mu\bar{u}}{h}wx-\dfrac{q_{\mathrm{a}}x}{h\varepsilon\varepsilon_0}\displaystyle\int_{-\frac{h}{2}}^{\frac{h}{2}}\rho_{\mathrm{q}}dy=\frac{d}{dt}\left(\rho_{\mathrm{m}}whx\bar{u}\right) \\ -\dfrac{q_{\mathrm{a}}\bar{\lambda}}{\varepsilon\varepsilon_0}+\bar{u}w\displaystyle\int_{-\frac{h}{2}}^{\frac{h}{2}}\left(\frac{3}{2}-6\frac{y^2}{h^2}\right)\rho_{\mathrm{q}}dy=\frac{d}{dt}q_{\mathrm{a}} \end{cases} \tag{10}$$

The system of nonlinear ordinary differential equations (10) cannot be solved analytically. However, an asymptotic solution can be found. The asymptotic solution is expressed in the form similar to Washburn's formula, with apparent viscosity μ_{a},

$$x=\left[\frac{\sigma\cos\theta h}{3\mu_{\mathrm{a}}}t\right]^{1/2} \tag{11}$$

where the relative viscosity change is defined as

$$\frac{\Delta\mu}{\mu}=\frac{\mu_{\mathrm{a}}-\mu}{\mu}=\eta\frac{\tanh\left(\frac{\kappa h}{2}\right)\left[\kappa h-2\tanh\left(\frac{\kappa h}{2}\right)\right]}{\left[1+\frac{\zeta e}{kT}\frac{\nu_{-}-\nu_{+}}{\nu_{-}+\nu_{+}}\frac{2\tanh\left(\kappa h/2\right)}{\kappa h}\right]\left(\kappa h\right)^2}\times100\% \tag{12}$$

where $\eta=\dfrac{4\varepsilon\varepsilon_0N_{\mathrm{A}}\zeta^2e^2}{\mu\Lambda_{\mathrm{m}}kT}$ is a dimensionless parameter.

With solutions in which two species of ions have comparable diffusivities (i.e. NaCl), Eq. (12) can be further simplified to

$$\frac{\Delta\mu}{\mu}=\eta\frac{\tanh\left(\frac{\kappa h}{2}\right)\left[\kappa h-2\tanh\left(\frac{\kappa h}{2}\right)\right]}{\left(\kappa h\right)^2}\times100\% \tag{13}$$

Figure 2 presents the relative viscosity change predicted by Eq. (13), in comparison to the values reported by Mortensen and Kristensen [33], under the same condition.

Capillary Filling in Closed-End Nanochannels

Figure 1 b illustrates the capillary filling process in a closed-end nanochannel. Both trapped air and filling liquid are considered as continua. Condensation of the liquid phase and dissolution of the gas phase are neglected. The forces governing the filling process of a closed-end nanochannel are the capillary force F_{s}, the viscous force F_{v}, and the resistance force of the trapped and compressed air,

$$F_{\mathrm{P}}=-hwp_0x/\left(L-x\right) \tag{14}$$

where L is the total length of the nanochannel and p_0 is the initial pressure of the trapped air. The electroviscous effect is not considered in this model. Since inertia force is negligible in nanoscale, the force balance $F_s + F_v + F_p = 0$ leads to

$$\frac{dx}{dt} = \frac{h\sigma\cos\theta}{6\mu x} - \frac{h^2 p_0}{12\mu(L-x)} \tag{15}$$

The parameters of Eq. (15) are made dimensionless as $x^* = x/L$, $t^* = t/2\tau$ and $\alpha = hp_0/2\sigma\cos\theta$, where α represents the ratio of force due to the trapped air pressure over the capillary force, and $\tau = 3\mu L^2/h\sigma\cos\theta$ is the required time to fill an open-end channel of the same length L. The governing equation (15) has then the dimensionless form

$$\frac{dx^*}{dt^*} = \frac{1}{x^*} - \frac{\alpha}{1-x^*} \tag{16}$$

Integrating the preceding equation with the initial condition $t^*(0) = 0$ for any $x_0^* < 1/(1+\alpha)$ leads to the relationship:

$$t^*(x^*) = \frac{x^{*2}}{2(1+\alpha)} - \frac{\alpha x^*}{(1+\alpha)^2} - \frac{\alpha}{(1+\alpha)^3}\ln\left[1-(1+\alpha)x^*\right] \tag{17}$$

The final position of the liquid column can be derived from Eq. (17) as:

$$\lim_{t^*\to\infty} x^* = \frac{1}{1+\alpha} \tag{18}$$

If condensation and dissolution are neglected, the filling length x of the liquid cannot exceed $L/(1+\alpha)$. At this final length, the magnitude of the resistance force of the trapped air is equal to that of the capillary force, $F_s + F_p = 0$. For the case of 45-nm-height nanochannels, the Laplace pressure caused by ethanol is approximately 9.96 bars.

EXPERIMENTS

Fabrication and Experimental Setup

Figure 3 depicts the schematic designs of the open-end and closed-end nanochannels under investigation. Nanochannels of 10 μm width and 45 nm and 80 nm depth were fabricated in silicon by reactive ion etching (RIE). The length of closed-end nanochannels ranges from 10 μm to 8 mm. For each channel dimension, a set of 10 channels were designed for obtaining good statistics in later experiments. Microchannels with a cross section of 8 μm×100 μm, which connected to the nanochannels, were realized by deep reactive ion etching (DRIE). Both ends of the microchannels are accessible through 1-mm-diameter reservoirs etched through the silicon wafer using a long DRIE process. Lastly, a Pyrex glass plate was anodically

bonded to the silicon wafer to seal the nanochannels. Bonding was performed at 350 ℃ and 400 V. Figure 4 a shows the fabricated channel network consisting of the access hole, the microchannel and the nanochannels. A typical filling process of open-end nanochannels is shown in Figure 4b.

In our experiments, nanochannels with reservoirs facing up were observed and recorded with an inverted microscope (Zeiss Observer D1) and a camera (EMCCD AndorIQ, Andor Technology PLC, Northern Ireland). The liquid (ethanol or isopropanol) was introduced into one of the reservoirs and filled the microchannel and nanochannels by capillary force. To keep ethanol from wetting the outer surface of the chip, a spacer made of polydimethylsiloxane (PDMS) was placed above the reservoir. The data were recorded as 16-bit gray-scale multi-images uncompressed tagged image files (TIF) with a size of 1004 pixels ×1002 pixels. The temperature and relative humidity were measured before each experiment. The surface tension and viscosity were derived from the temperature, using a formula provided by Yaws [61]. The environmental temperature during the experiments for both cases of with ethanol and isopropanol is measured as $26 \pm 1\ ^{o}\mathrm{C}$. The relative humidity of the environment was 48%. According to the formula provided by [61], the relative variation in surface tension and viscosity is less than 1%, which is considered to be negligible. Macroscopic contact angle measurement revealed that both liquids under investigation totally wet silicon and glass ($\theta = 0°$).

In the experiment with closed-end nanochannels, the filling processes were observed with different magnifications and time scales. The experiment consists of two steps. In the first step, we recorded the filling process from the entrance of the nanochannels until the end of the 3-mm-long channel set. Objective lens with a magnification of 2.5× was used for this purpose. The field of view was approximately 3 mm × 3 mm. The exposure time was 10 ms. Images were recorded with a frame rate of 17 fps. In the second step, one of the closed ends of the nanochannels was chosen to investigate the behavior of the advancing meniscus and of the trapped air. A magnification of 20× and a frame rate of 5 fps were used for this experiment. The images were recorded to observe the slow process of condensation and dissolution until the nanochannels were fully filled.

Experiment Result

The square of filling distance versus time characteristics, as shown in Figure 5, reveals that capillary filling in open-end nanochannels qualitatively follows Washburn's formula

$$x = \left[\frac{\sigma \cos\theta h}{3\mu} t \right]^{1/2} \tag{19}$$

However, quantitative analysis shows that the Washburn coefficient,

$$a = \sqrt{\frac{\sigma \cos\theta h}{3\mu}} \tag{20}$$

is lower than predicted by the classical Washburn's theory, which is equivalent to an increase in apparent viscosity. Table 1 lists the measured relative viscosity change of ethanol and isopropanol. It is reported in recent investigations that electroviscous effect is the cause of reduction of speed in pressure-driven flow and even capillary filling [32-35]. However, as derived from Eq. (13), which indicates that the dimensionless parameter η is on the order of unity for most of electrolytic solutions (i.e., $\eta \approx 0.5$ for NaCl 0.01*M* solution), the maximum increase in apparent viscosity is not more than 5%. In our capillary filling experiment, non-electrolytic liquids that exhibit negligible electroviscous effect also encounter a relatively high viscosity increase ratio, as shown in Table 1. Therefore, there are other phenomena besides the electroviscous effect that cause the increase in apparent viscosity of liquid in nanochannels. There are reports on the formation of air bubbles during the filling process [8-11]. A fraction of energy is stored in term of surface energy of the air bubbles. Hence, less energy transfers into kinetic energy of the fluid column, leading to the reduction in filling speed. Additionally, the presence of bubbles modifies the flow profile and may lead to an increase in viscous dissipation, and thus to a slower filling.

Figure 6a shows the measured filling length of isopropanol in closed-end nanochannels with different lengths. The graph shows an identical filling pattern for all nanochannels with different lengths in the first stage. When the meniscus of the liquid approaches the end of the channel, the filling process begins to slow down. Figure 6b depicts the normalized filling length as a function of normalized time in comparison to the theoretical behavior predicted by Eq. (17) with the bulk value of viscosity. The results show that the filling speed in the first stage is actually lower than predicted by theory. This behavior was also observed in previous works on capillary filling of open-end nanochannels. The phenomenon is described by introducing an apparent viscosity, whose value is higher than the bulk value. Figure 6 c presents a comparison to amended theory using modified apparent viscosity, obtained by fitting the first stage of filling to the Washburn's formula. Corresponding results for ethanol are presented in Figure 7.

The results show that the filling process consists of two major stages. In the initial stage, the length of the liquid column follows the theory well, but with a higher apparent viscosity. In this stage, where $t^* << \tau$, the pressure force is negligible and the filling process can be approximated by Washburn's law. This condition is used to calculate the experimental relative viscosity change, as presented in

Table 2. The relative viscosity change in closed-end nanochannels is noticeably higher than those in the open-end nanochannel. The difference is more significant for shorter channels. This effect can be explained by the non-ideality of the assumptions used in the mathematical model. In this model, an isothermal condition is used. However, if the dissipation of heat is not fast enough, the compression of air during the filling process may cause heating of air, and hence increase the pressure force reducing the filling speed. In the second stage, the meniscus does not stop as assumed with the theory. The liquid column slowly advances toward the end of the nanochannel and finally fills it completely. We observed that in the second stage, the filling process consists of a combination of condensation of the liquid phase and dissolution of the gas phase.

A larger noise was detected in the second stage of the filling process because of the irregular shape of filled areas. To analyze this second stage, we evaluated the remaining unfilled area of the nanochannel. Images of the end of the nanochannels recorded at a higher magnification of 20× were analyzed. Figure 8 a shows the measured surface area of the unfilled part in a 2-mm-long nanochannel as a function of time. The measured data were filtered by Savitzky-Golay filter of second order to reduce the noises. These two stages can be observed clearly in Figure 8a. In the second stage the amount of unfilled area reduces linearly with time. This linear behavior is confirmed by Figure 8b, which plots the rate of change of the unfilled area as a function of time. The inserts in Figure 8a show that during the first stage, the meniscus of the liquid advances more quickly and the shape of the meniscus is more defined. In the second stage, the filling speed is much slower and the meniscus does not have a defined shape. We observed that liquid islands were formed and air bubbles were trapped in the confined space. While the liquid islands spread, the encircled bubbles reduced their size and gradually disappeared. This phenomenon can be considered as a combination of gas dissolution and liquid condensation and probably is enhanced by film flows and corner flows [25]. The advance movement of the meniscus in the second stage is governed by the dissolution of gas into liquid and the diffusion of the gas molecules out of the nanochannels. Due to the high pressure of the trapped gas, which is approximately equal to the Laplace pressure, the gas molecules dissolve into the liquid phase, and the concentration of gas molecules at the meniscus in the liquid phase is determined by the Henry's law. Due to the difference in gas molecules concentration between the meniscus and the entrance of the nanochannel, the gas molecules diffuse out of the channel. The diffusion rate of the gas molecules determines the advancing rate of the meniscus. A detailed theoretical analysis on this phenomenon is beyond the scope of this article and is considered in our future works. The evaporation and condensation of liquids is properly due to thermal fluctuation. These phenomena lead to the formation of liquid islands and air bubbles, which cause local instability of the meniscus in the second stage. However, because the diffusion process only depends on the global concentration gradient in the nanochannel, local instability caused by evaporation and condensation should not affect the average advancing rate of the meniscus.

CONCLUSIONS

This article reports the theoretical and experimental results on capillary filling in open-end and closed-end nanochannels. The nanochannels of 45 nm and 80 nm depths and 10 μm width were fabricated by a standard plasma etching process in silicon wafer. A Pyrex glass cover was anodically bonded to the silicon wafer to seal the nanochannels. The nanochannels were then filled with non-electrolytic liquid. The filling processes were observed and recorded. A mathematical model to calculate the electroviscous effect was established. This model shows that contribution of electroviscous effect in the reduction of filling speed is small. The result agrees well with previous theoretical works on the electroviscous effect. Consequently, there exists other phenomena involve in the variation in Washburn's coefficient, such as the formation of air bubbles. The capillary filling processes of closed-end nanochannels were also recorded and compared to a simple theoretical model that neglects the condensation of the liquid and the dissolution of gas. The data show clearly two stages of the filling process. In the first stage, the experimental data agree well with the theory, but with a higher apparent viscosity. However, in the second stage, the menisci do not stop at the critical position predicted by the theory, but continue to fill until the end of the nanochannels. A quantitative analysis of this stage shows a linear relationship between the filling area and the time. High-magnification images reveal that in this stage liquid islands form, while gas bubbles trapped in the nanochannels dissolve into the liquid. The air bubbles reduce their size before totally disappearing. This phenomenon suggests that condensation of liquid and dissolution of gas are important processes at the nanoscale, where the Laplace pressure is relatively high. The observed condensation and dissolution phenomena can affect transport processes of liquid in nanochannels.

NOMENCLATURES

a	Washburn's coefficient
A	Area of trapped air
A_c	Cross-sectional area of the channel
DRIE	Deep reactive ion etching
e	Elementary charge, 1.305×10^{-19}C
EDL	Electric double layer
F_e	Electrical force
F_s	Surface force, capillary force
F_v	Viscous drag force
F_p	Pressurized force of trapped air

h	Channel height
k	Boltzmann's constant, $1.381\times10^{-23}\,JK^{-1}$
L	Channel length
n	Local concentration
n^0	Bulk concentration
N_A	Avogadro's number, 6.0221415×10^{23}
p_0	Pressure
p_0	Initial (atmospheric) pressure
q_a	Accumulated charge
t	Time variable
t^*	Dimensionless time
T	Room temperature
u	Fluid velocity
U_S	Streaming potential
w	Channel width
x	Capillary filling length
x^*	Dimensionless filling length
x_0^*	Initial dimensionless filling length
y	Coordinate across the channel height
z	Charge number

Greek Symbols

α	Ratio between initial pressure and Laplace pressure
$\Delta\mu$	Increase in dynamic viscosity
ε	Relative permittivity of the fluid
ε_0	Permittivity of free space, $8.854\times10^{-12}\mathrm{CV^{-1}m^{-1}}$
ζ	Zeta potential
η	Material dimensionless parameter
θ	Contact angle

κ	Inverse of Debye thickness
λ	Conductivity of the fluid
Λ_m	Molar conductivity of solution
μ	Dynamic viscosity
μ_a	Apparent dynamic viscosity
σ	Surface tension
ρ_m	Mass density of the fluid
ρ_q	Charge density
τ	Characteristic filling time
υ	Ion mobility
Ψ	Electrostatic potential across the channel's height

Subscripts

0	initial condition
+	positive ion
-	negative ion
a	apparent, accumulated
c	cross section
E	electric
m	molar, mass
p	pressurized
q	charge
s	surface
S	streaming
v	viscous

Superscripts

‾	Average value across the height
^	Divide by channel width w
$_i$	Belong to ion species i

REFERENCES

[1] Kandlikar, S.G., and Grande, W.J., Evaluation of single phase flow in microchannels for high heat flux chip cooling-thermohydraulic performance enhancement and fabrication technology, *Heat Transfer Engineering*, vol. 25, no. 8, pp. 5-16, 2004.

[2] Cheng, L., Bandarra Filho, E.P., and Thome J.R., Nanofluid two-phase flow and thermal physics: A new research frontier of nanotechnology and its challenges, *Journal of Nanoscience and Nanotechnology*, vol. 8, no.7, pp. 3315-3332, 2008.

[3] Roday, A.P., and Jensen M.K., A review of the critical heat flux condition in mini- and microchannels, *Journal of Mechanical Science and Technology*, vol. 23, no.9 , pp. 2529-2547, 2009.

[4] Weisberg, A., Bau, H.H., and Zemel, J.N., Analysis of microchannels for integrated cooling, *International Journal of Heat and Mass Transfer*, vol. 35, no. 10, pp. 2465-2474, 1992.

[5] Peng, X.F., and Wang, B.X., Forced convection and flow boiling heat transfer for liquid flowing through microchannels, *International Journal of Heat and Mass Transfer*, vol. 36, no.14, pp. 3421-3427, 1993.

[6] Peng, X.F., and Peterson, G.P., The effect of thermofluid and geometrical parameters on convection of liquids through rectangular microchannels, *International Journal of Heat and Mass Transfer*, vol. 38, no. 4, pp. 755-758, 1995.

[7] Peng, X.F., Wang, B.X., Peterson, G.P., and Ma, H.B., Experimental investigation of heat transfer in flat plates with rectangular microchannels, *International Journal of Heat and Mass Transfer*, vol. 38, no. 1, pp. 127-137, 1995.

[8] Peng X.F., and Peterson, G.P., Convective heat transfer and flow friction for water flow in microchannel structures, *International Journal of Heat and Mass Transfer*, vol. 39, no. 12, pp. 2599-2608, 1996.

[9] Hetsroni, G., Mosyak, A., and Segal, Z., Nonuniform temperature distribution in electronic devices cooled by flow in parallel microchannels, *IEEE Transactions on Components and Packaging Technologies*, vol. 24, no. 1, pp. 16-23, 2001.

[10] Schubert, K., Brandner, J., Fichtner, M., Linder, G., Schygulla, U., and Wenka, A., Microstructure devices for applications in thermal and chemical process engineering, *Microscale Thermophysical Engineering*, vol. 5, no. 1, pp. 17-39, 2001.

[11] Zhang, J., Tan, K.L., Hong, G.D., Yang, L.J., and Gong, H.Q., Polymerization optimization of SU-8 photoresist and its applications in microfluidic systems and

MEMS, *Journal of Micromechanics and Microengineering*, vol. 11, no. 1, pp. 20-26, 2001.

[12] Kawaji, M., and Chung, P.M.Y., Adiabatic gas-liquid flow in microchannels, *Microscale Thermophysical Engineering*, vol. 8, no. 3, pp. 239-257, 2004.

[13] Kang, M. K., Shin, J. H., Lee, H. H., and Chun, K., Analysis of laminar convective heat transfer in micro heat exchanger for stacked multi-chip module, *Microsystem Technologies*, vol. 11, no. 11, pp. 1176-1186, 2005.

[14] Ohta H., Boiling and two-phase flow in channels with extremely small dimensions: A review of Japanese research, *Microfluidics and Nanofluidics*, vol. 1, no. 2, pp. 94-107, 2005.

[15] Rosa P., Karayiannis, T.G., and Collins, M.W., Single-phase heat transfer in microchannels: The importance of scaling effects, *Applied Thermal Engineering*, vol. 29, no. 17-18, pp. 3447-3468, 2009.

[16] Eijkel, J.C.T., and Van Den Berg, A., Nanofluidics: What is it and what can we expect from it?, *Microfluidics and Nanofluidics*, vol. 1, no. 3, pp. 249-267, 2005.

[17] Mijatovic, D., Eijkel, J.C.T., and Van Den Berg, A., Technologies for nanofluidic systems: Top-down vs. bottom-up - A review, *Lab on a Chip - Miniaturisation for Chemistry and Biology*, vol. 5, no. 5, pp. 492-500, 2005.

[18] Perry, J.L., and Kandlikar, S. G., Review of fabrication of nanochannels for single phase liquid flow, *Microfluidics and Nanofluidics*, vol. 2, no. 3, pp. 185-193, 2006.

[19] Yuan Z., Garcia, A.L., Lopez, G.P., and Petsev, D.N., Electrokinetic transport and separations in fluidic nanochannels, *Electrophoresis*, vol. 28, no. 4, pp. 595-610, 2007.

[20] Abgrall, P., Low, L.N., and Nguyen, N.T., Fabrication of planar nanofluidic channels in a thermoplastic by hot-embossing and thermal bonding, *Lab on a Chip - Miniaturisation for Chemistry and Biology*, vol. 7, no. 4, pp. 520-522, 2007.

[21] Abgrall, P., and Nguyen, N.T., Nanofluidic devices and their applications, *Analytical Chemistry*, vol. 80, no. 7, pp. 2326-2341, 2008.

[22] Nguyen, N.T., and Truong, T.Q., A fully polymeric micropump with piezoelectric actuator, S*ensors and Actuators, B: Chemical*, vol. 97, no. 1, pp. 137-143, 2004.

[23] Nguyen, N.T., and White, R.M., Acoustic streaming in micromachined flexural plate wave devices: numerical simulation and experimental verification, *IEEE*

Transactions on Ultrasonics, Ferroelectrics, and Frequency Control, vol. 47, no. 6, pp. 1463-1471, 2000.

[24] Truong, T.Q., and Nguyen, N.T., A polymeric piezoelectric micropump based on lamination technology, *Journal of Micromechanics and Microengineering*, vol. 14, no. 4, pp. 632-638, 2004.

[25] Eijkel, J. C. T., Dan, B., Reemeijer, H.W., Hermes, D.C., Bomer, J.G., and Van Den Berg, A., Strongly accelerated and humidity-independent drying of nanochannels induced by sharp corners, *Physical Review Letters*, vol. 95, no. 25, art. no. 256107, pp. 1-4, 2005.

[26] Han, A., Mondin, G., Hegelbach, N.G., de Rooij, N.F., and Staufer, U., Filling kinetics of liquids in nanochannels as narrow as 27 nm by capillary force, *Journal of Colloid and Interface Science*, vol. 293, no. 1, pp. 151-157, 2006.

[27] Persson, F., Thamdrup, L.H., Mikkelsen, M.B.L., Jaarlgard, S.E., Skafte-Pedersen, P., Bruus, H., and Kristensen, A., Double thermal oxidation scheme for the fabrication of SiO_2 nanochannels, *Nanotechnology*, vol. 18, no. 24, art. no. 245301, 2007.

[28] Tas, N.R., Haneveld, J., Jansen, H.V., Elwenspoek, M., and van den Berg, A., Capillary filling speed of water in nanochannels, *Applied Physics Letters*, vol. 85, no. 15 , pp. 3274-3276, 2004.

[29] Thamdrup, L. H., Persson, F., Bruus, H., Kristensen, A., and Flyvbjerg, H., Experimental investigation of bubble formation during capillary filling of SiO_2 nanoslits, *Applied Physics Letters*, vol. 91, no. 16, art. no. 163505, pp. 1-3, 2007.

[30] Nguyen, N.T., and Huang X.Y., Thermocapillary effect of a liquid plug in transient temperature fields, *Japanese Journal of Applied Physics, Part 1: Regular Papers and Short Notes and Review Papers*, vol. 44, no. 2, pp. 1139-1142, 2005.

[31] van Honschoten, J.W., Escalante, M., Tas, N.R., Jansen, H.V., and Elwenspoek, M., Elastocapillary filling of deformable nanochannels, *Journal of Applied Physics*, vol. 101, no. 9, art. no. 094310, pp. 1-7, 2007.

[32] Huang, K.D., and Yang, R.J., Electrokinetic behaviour of overlapped electric double layers in nanofluidic channels, *Nanotechnology*, vol. 18, no. 11, art. no. 115701, pp. 1-6, 2007.

[33] Mortensen, N.A., and Kristensen, A., Electroviscous effects in capillary filling of nanochannels, *Applied Physics Letters*, vol. 92, no. 6, art. no. 063110, pp. 1-3, 2008.

[34] Ren, C.L., and Li, D., Improved understanding of the effect of electrical double layer on pressure-driven flow in microchannels, *Analytica Chimica Acta*, vol. 531, no. 1, pp. 15-23, 2005.

[35] Yang, C., and Li, D., Electrokinetic effects on pressure-driven liquid flows in rectangular microchannels, *Journal of Colloid and Interface Science*, vol. 194, no. 1, pp. 95-107, 1997.

[36] Shaw, T. M., Drying as an immiscible displacement process with fluid counterflow, *Physical Review Letters*, vol. 59, no. 15, pp. 1671-1674, 1987.

[37] Prat, M., Percolation model of drying under isothermal conditions in porous media, *International Journal of Multiphase Flow*, vol. 19, no. 4, pp. 691-704, 1993.

[38] Yiotis, A.G., Boudouvis, A.G., Stubos, A.K., Tsimpanogiannis, I.N., and Yortsos, Y.C., Effect of liquid films on the isothermal drying of porous media, *Physical Review - Statistical, Nonlinear, and Soft Matter Physics*, vol. 68, no. 32, art. no. 037303, pp. 1-4, 2003.

[39] Yang, J., Lu, F., and Kwok, D.Y., Dynamic interfacial effect of electroosmotic slip flow with a moving capillary front in hydrophobic circular microchannels, *Journal of Chemical Physics*, vol. 121, no. 15, pp. 7443-7448, 2004.

[40] Chakraborty, D., and Chakraborty, S., Interfacial phenomena and dynamic contact angle modulation in microcapillary flows subjected to electroosmotic actuation, *Langmuir*, vol. 24, no. 17, pp. 9449-9459, 2008.

[41] Chakraborty, S., Electroosmotically driven capillary transport of typical non-Newtonian biofluids in rectangular microchannels, *Analytica Chimica Acta*, vol. 605, no. 2, pp. 175-184, 2007.

[42] Chakraborty, S., and Mittal, R., Droplet dynamics in a microchannel subjected to electrocapillary actuation, *Journal of Applied Physics*, vol. 101, no. 10, art. no. 104901, pp. 1-8, 2007.

[43] Huang, W., Bhullar, R.S., and Yuan, C.F., The surface-tension-driven flow of blood from a droplet into a capillary tube, *Journal of Biomechanical Engineering*, vol. 123, no. 5, pp. 446-454, 2001.

[44] Chakraborty, S., Dynamics of capillary flow of blood into a microfluidic channel, *Lab on a Chip - Miniaturisation for Chemistry and Biology*, vol. 5, no. 4, pp. 421-430, 2005.

[45] Kundu, P. K., *Fluid mechanics*, 3rd ed., Elsevier Academic Press, Amsterdam,1990.

[46] Phan, V.N., Yang, C., and Nguyen, N.T., Analysis of capillary filling in nanochannels with electroviscous effects, *Microfluidics and Nanofluidics*, vol. 7, no. 4, pp. 1-12, 2009.

[47] Debye, P., and Hückel, E., The theory of electrolytes. I. Lowering of freezing point and related phenomena, *Physikalische Zeitschrift*, vol. 24, no. 1, pp. 185–206, 1923.

[48] Yuan, Z., Garcia, A.L., Lopez, G.P., and Petsev, D.N., Electrokinetic transport and separations in fluidic nanochannels, *Electrophoresis*, vol. 28, no. 4, pp. 595-610, 2008.

[49] Conlisk, A.T., The Debye-Hückel approximation: Its use in describing electroosmotic flow in micro- and nanochannels, *Electrophoresis*, vol. 26, no. 10, pp. 1896-1912, 2005.

[50] Bowen, W.R., and Jenner, F., Dynamic ultrafiltration model for charged colloidal dispersions: a Wigner-Seitz cell approach, *Chemical Engineering Science*, vol. 50, no. 11, pp. 1707-1736, 1995.

[51] Burgreen, D., and Nakache, F.R., Electrokinetic flow in ultrafine capillary slits, *Journal of Physical Chemistry*, vol. 68, no. 5, pp. 1084-1091, 1964.

[52] Hsu, J.P., Kao, C.Y., Tseng, S., and Chen, C.J., Electrokinetic flow through an elliptical microchannel: Effects of aspect ratio and electrical boundary conditions, *Journal of Colloid and Interface Science*, vol. 248, no. 1, pp. 176-184, 2002.

[53] Hunter, R.J., *Zeta Potential in Colloid Science: Principles and Applications*, Academic Press: London, 1981.

[54] Levine, S., Marriott, J.R., Neale, G., and Epstein, N., Theory of electrokinetic flow in fine cylindrical capillaries at high zeta-potentials, *Journal of Colloid and Interface Science*, vol. 52, no. 1, pp. 136-149, 1975.

[55] Levine, S., Marriott, J.R., and Robinson, K., Theory of electrokinetic flow in a narrow parallel-plate channel, *Journal of the Chemical Society, Faraday Transactions 2: Molecular and Chemical Physics*, vol. 71, no. 1, pp. 1-11, 1975.

[56] Levine, S., and Neale, G.H., The prediction of electrokinetic phenomena within multiparticle systems. I. Electrophoresis and electroosmosis, *Journal of Colloid and Interface Science*, vol. 47, no. 2, pp. 520-529, 1974.

[57] Rice, C.L., Whitehead, R., Electrokinetic Flow in a Narrow Cylindrical Capillary, *Journal of Physical Chemistry*, vol. 69, no. 11, pp. 4017-4023, 1965.

[58] Russel, W.B., Saville, D.A., and Schowalter, W.R., *Colloidal Dispersions*, Cambridge University Press, London, 1989.

[59] Verwey, E.J.W., and Overbeek, J.T.G., *Theory and Stability of Lyophobic Colloids*, Elsevier, Amsterdam, 1948.

[60] Phan, V.N., Yang, C., and Nguyen, N.T., Analysis of capillary filling in nanochannels with electroviscous effects, *Microfluidics and Nanofluidics*, vol. 7, no. 4, pp. 519-530, 2009.

[61] Yaws, C. L., *Thermal Physical Properties*, William Andrew, New York, 2008.

Table 1 Relative viscosity change of different fluids and channel geometries.

Fluid	Channel height (nm)	Relative viscosity change (%)	
		Mean	Std dev
Isopropanol	45	28.0	6.10
Isopropanol	80	9.70	1.00
Ethanol	45	21.5	2.00
Ethanol	80	9.30	3.60

Table 2 Ratio between the increase in viscosity to standard value for different fluids and channel geometries during the first stage of filling in closed-end nanochannel (45nm in height).

Fluid	Channel length (mm)	Relative viscosity change (%)
Isopropanol	0.5	140
Isopropanol	1	136
Isopropanol	1.5	92.0
Isopropanol	2	81.0
Isopropanol	2.5	77.0
Ethanol	0.5	149
Ethanol	1	115
Ethanol	1.5	108
Ethanol	2	108
Ethanol	2.5	103
Ethanol	3	95.0

LIST OF FIGURE

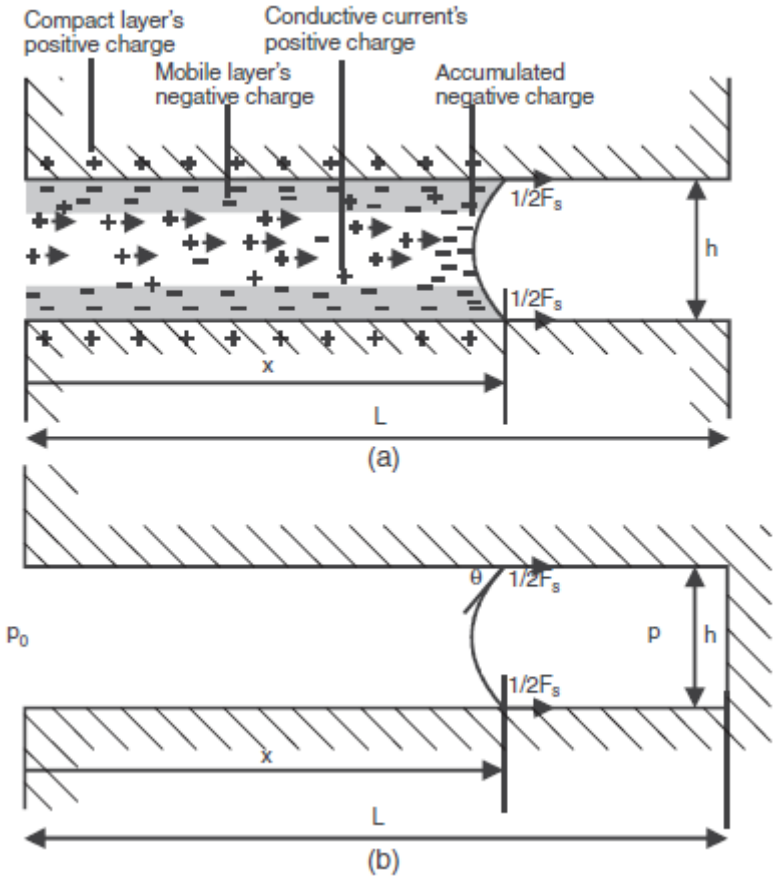

Figure 1 (a) Capillary filling in an open-end nanochannel: Ions distribution and movement inside a liquid column moving in a nanochannel due to capillary filling. (b) Capillary filling in a closed-end nanochannel

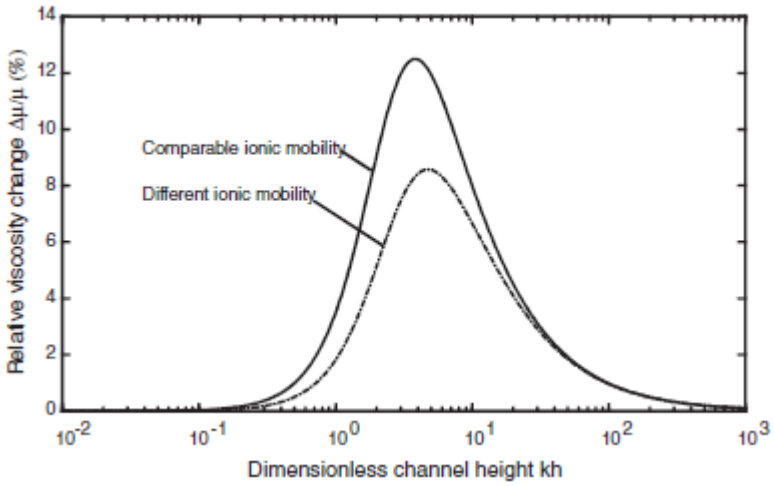

Figure 2 Relative viscosity change (Solid line: values predicted by the current theory. Dashed line: values reported by Mortensen and Kristensen)

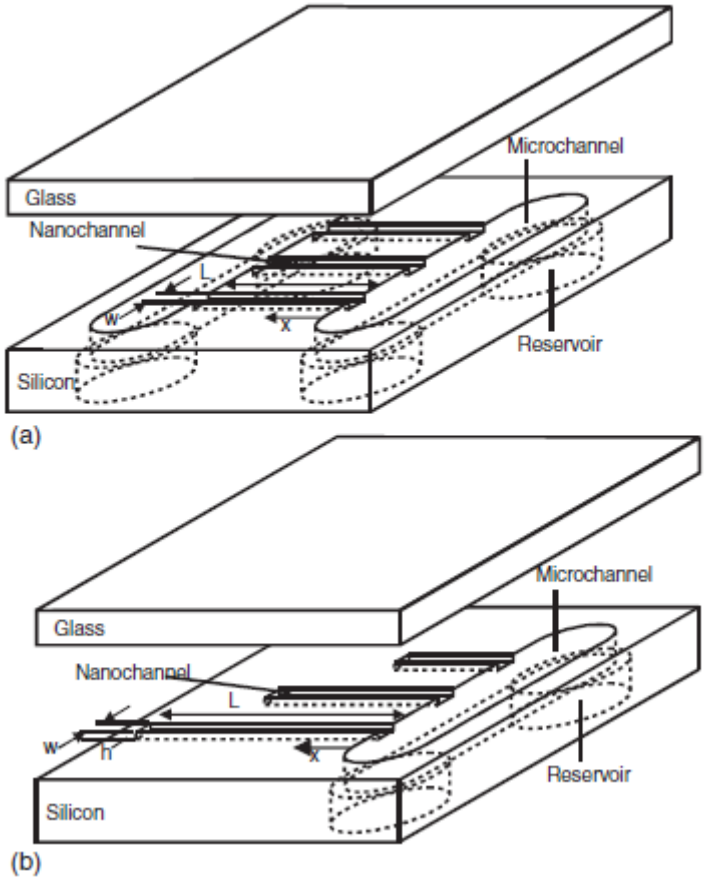

Figure 3 Schematic design of the test chip with nanochannels, microchannels and reservoirs etched in silicon: (a) open-end nanochannels; (b) closed-end nanochannels

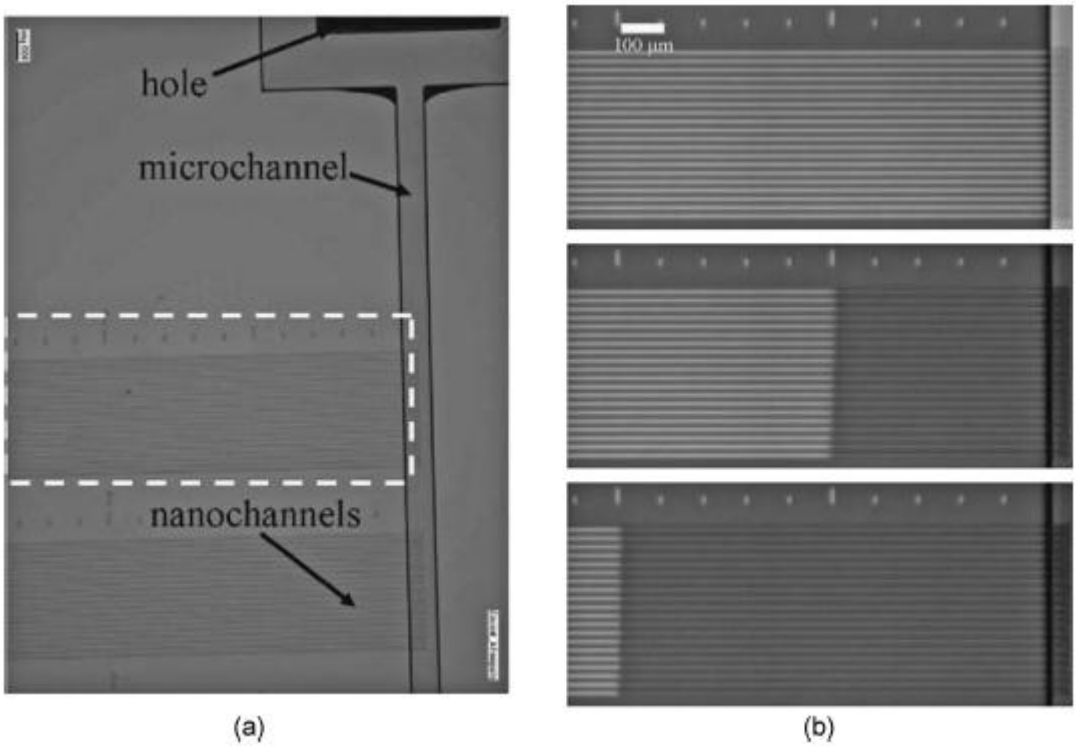

Figure 4 (a) The fabricated channel network. (b) Filling of liquid in nanochannels

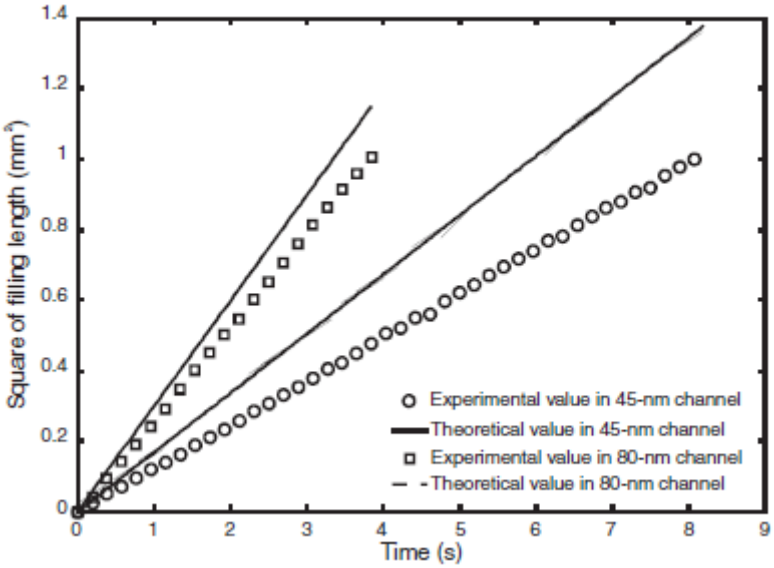

Figure 5 Square of filling length versus filling time in open-end nanochannels in a typical filling process of isopropanol in 45-nm and 80-nm nanochannels

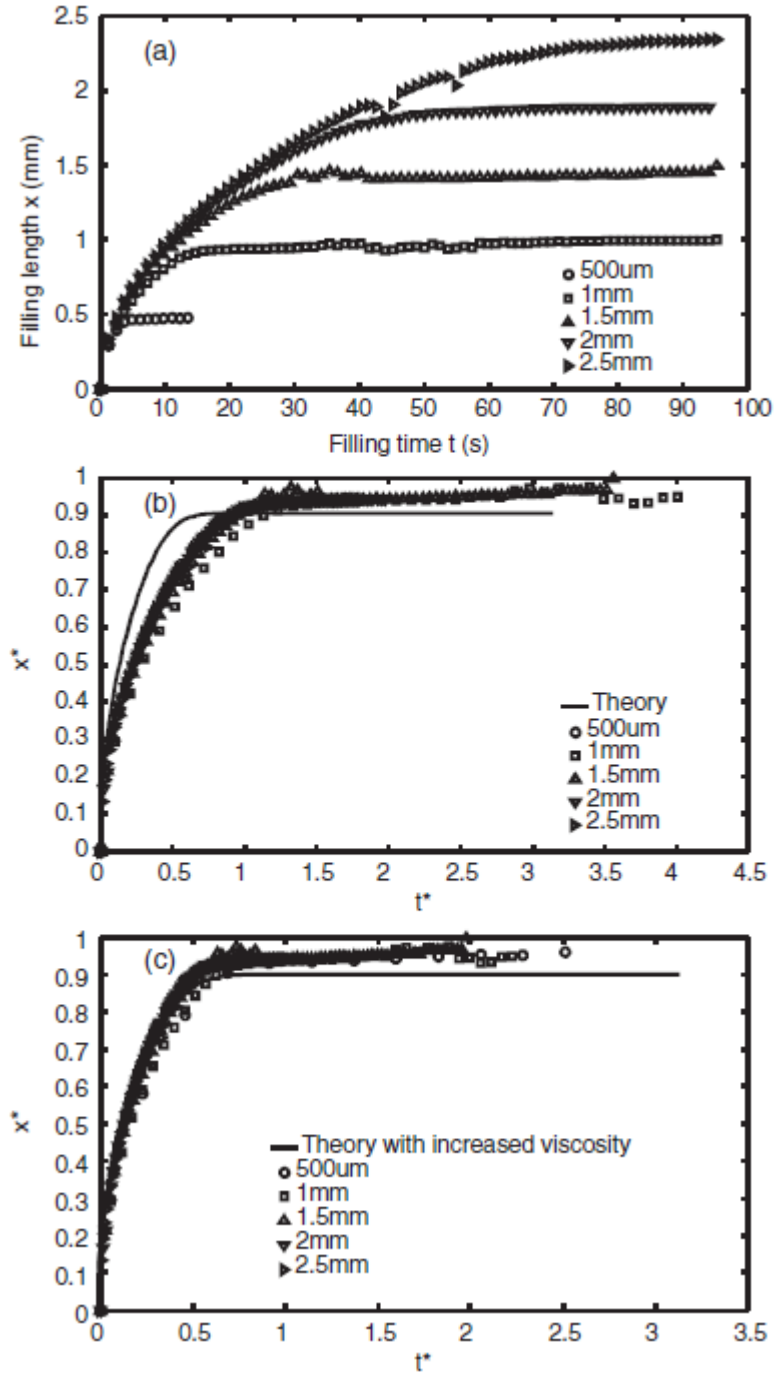

Figure 6 Filling process of isopropanol in closed-end nanochannels of different lengths, 45-nm depth and 10-μm width: (a) Filling length versus time; (b) Normalized filling length versus normalized time; (c) Normalized filling length versus normalized time with apparent viscosity $\mu_a = 1.8\mu$

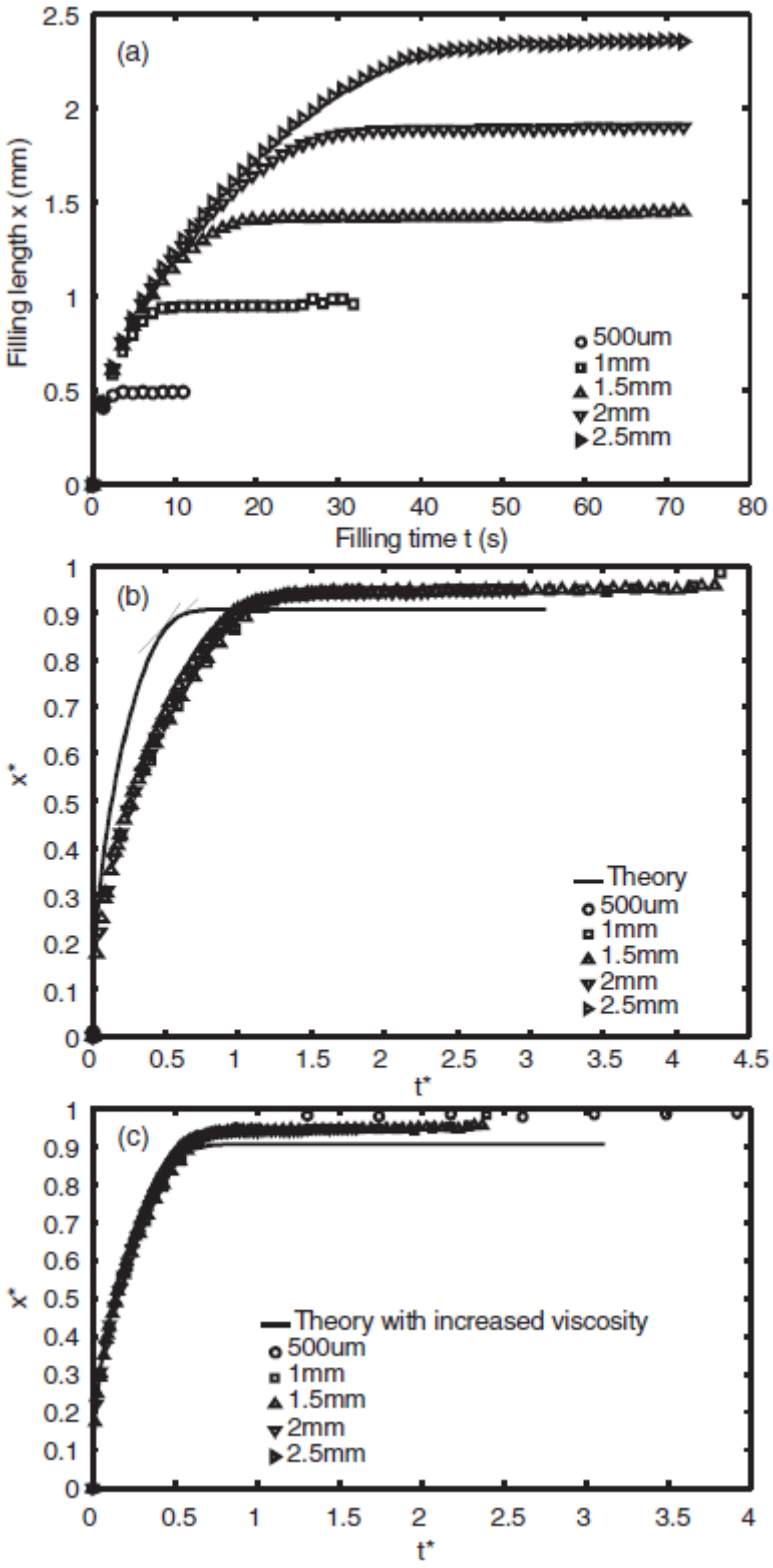

Figure 7 Filling process of ethanol in closed-end nanochannels of different lengths, 45-nm depth and 10-μm width: (a) Filling length versus time; (b) Normalized filling length versus normalized time; (c) Normalized filling length versus normalized time with apparent viscosity $\mu_a = 1.8\mu$

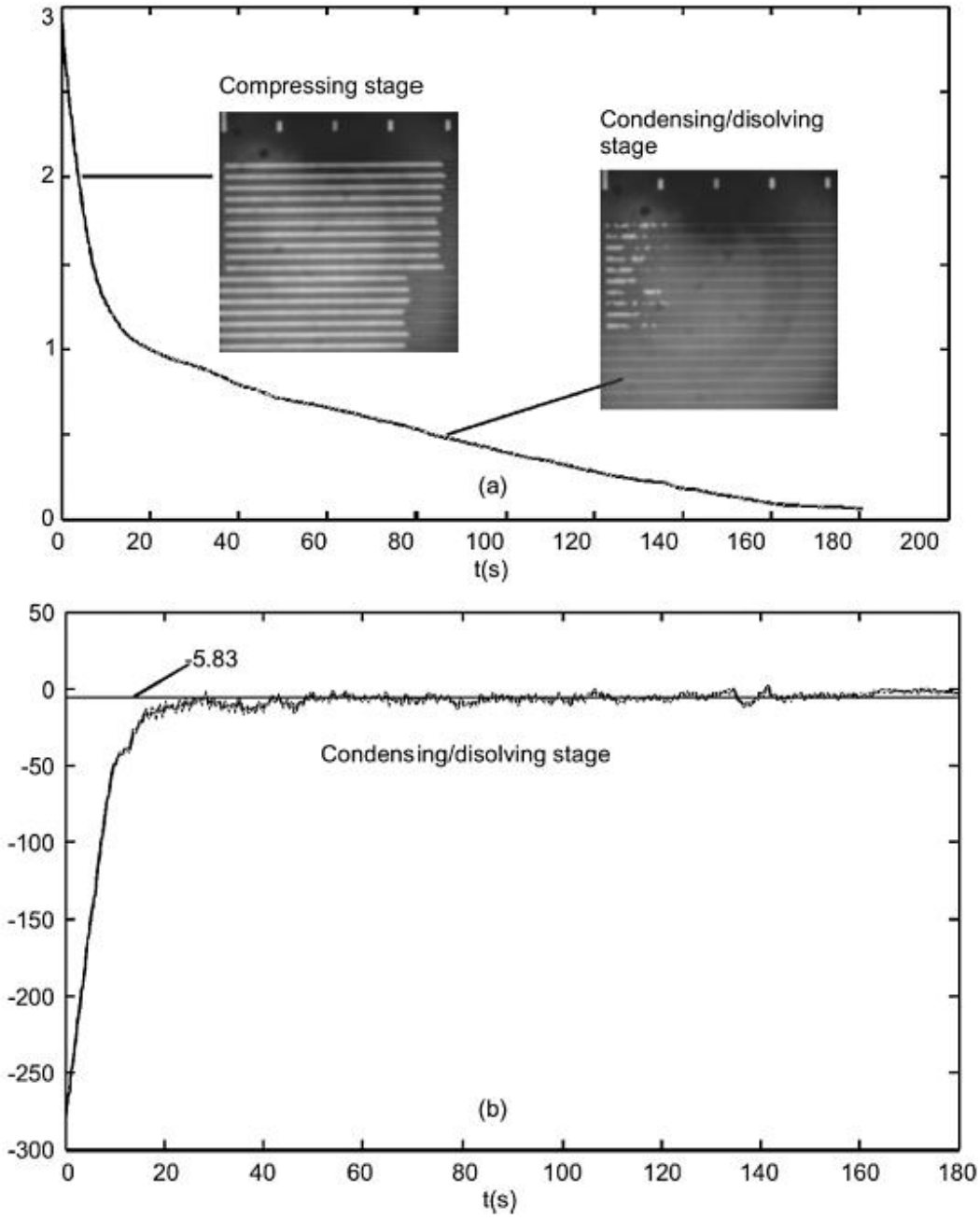

Figure 8 Final stage of capillary filling in closed-end nanochannels: (a) Surface area of the unfilled part at the end of a 2mm-long nanochannel as function of time (the starting time is arbitrary); (b) Rate of change of the surface area in (a)

AUTHORS

Vinh Nguyen Phan received his B.E. in 2006 from the School of Mechanical and Aerospace Engineering (MAE), Nanyang Technological University (NTU), Singapore. Currently, he is a Ph.D. student at MAE, NTU. His research interests are in nanoscale transport phenomena, especially capillary filling, evaporation, condensation, and multiphase flows.

Pierre Joseph received his Ph.D. in physics of liquids from University Pierre et Marie Curie in Paris (MMN laboratory, ESPCI) in 2005. In 2005-2007, he worked as a postdoctoral fellow in PMCN laboratory (CNRS-University Lyon 1, France) on flows along superhydrophobic surfaces. He is currently a CNRS research associate at LAAS-CNRS in Toulouse (France), working on nanofluidic technologies, instrumentation and flow control. He is co-author of a book chapter and several publications on microfluidics and nanofluidics.

Lyes Djeghlaf received his Dip. –Ing. in electronics in 2006, from University of Science and Technology USTHB, Algeria, and a master's diploma in micro and nano system from Paul Sabatier University Toulouse III, France, in 2009. In 2007 he worked as technical manager in Mzitec (company of import-export medical material, Algeria). Since January 2010 he has been a Ph.D. student in LAAS-CNRS (Toulouse,

France) working on the coupling between electrochemistry and microfluidics (electro chemical micro sensor, ChemFET).

Alaa El Dine Allouch received his master's diploma from Paul Sabatier University (Toulouse, France) in 2008, in the field of micro and nano systems. Since October 2008 he has been a Ph.D. student at LAAS-CNRS (Toulouse, France), working on the generation and control of bubbles and droplets generated inside micro- and nanochannels.

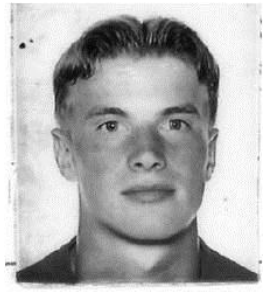

David Bourrier is an assistant engineer at LAAS-CNRS (Toulouse, France), a laboratory of the National Research Center. He works in the TEAM in charge of the facilities and the support development on MEMS research. His current research interests are in the areas of molds realization and electroplating. He works on the development of new photoresists and on electroplating optimization. He has coauthored 37 papers and a patent.

Patrick Abgrall is a postdoctoral researcher at the Biomedical Diagnostics Institute in Dublin. He earned his Ph.D. with a thesis on polymer fabrication for lab-on-chips at LAAS-CNRS in Toulouse, France. He was a member of the Singapore-MIT alliance, where his research was focused on the fabrication and applications of polymer nanofluidic devices.

Anne-Marie Gué studied physics at the National Institute for Applied Science and received her Ph.D. degree at the University of Toulouse, France. She joined LAAS-CNRS in 1988 as a CNRS senior scientist. Since 1994, she has been involved in the development of microtechnologies and microsystems for chemical and biological applications. She first worked in the design and fabrication of miniaturized chemical and biosensors. Her activity is now focusing on microfluidic aspects. She has been the head of the Microsystem and System Integration Group at LAAS-CNRS from 1999 to 2006, and has coauthored more than 90 articles and international communications, and 6 patents.

Chun Yang obtained his B.Sc. degree from the Department of Thermal Engineering at Tsinghua University in 1985, master's degree in engineering thermophysics from the University of Science and Technology of China in 1988, and Ph.D. degree in mechanical engineering from the University of Alberta in 1999. In 1999, he joined Nanyang Technological University, Singapore, and now is an associate professor in the School of Mechanical and Aerospace Engineering. He is the author and co-author of more than 100 publications in referred international journals, and has co-authored one textbook entitled *Elementary Electrokinetic Flow*. He serves as a member of the editorial advisory board for *Journal of Microfluidics and Nanofluidics* and *International Journal of Emerging Multidisciplinary Fluid Sciences*. He is a reviewer for the Research Grant Council of Hong Kong, Research Grant Council of Australia, National Science and Engineering Research Council of Canada, and Dutch Technology Foundation, and also a peer reviewer for more than 30 international journals.

Nam-Trung Nguyen received his Dip.-Ing., Dr. Ing., and Dr. Ing. Habil, degrees from Chemnitz University of Technology, Germany, in 1993, 1997, and 2004, respectively. In 1998, he worked as a postdoctoral research engineer in the Berkeley Sensor and Actuator Center (University of California–Berkeley). Currently, he is an associate professor with the School of Mechanical and Aerospace Engineering of the NTU in Singapore. His research is focused on microfluidics and instrumentation for biomedical applications. He has published a number of research papers on microfluidics. The first and second editions of his bestseller *Fundamentals and Applications of Microfluidics* co-authored with S.Wereley were published in 2002 and 2006, respectively. His latest book *Nanofluidics*, co-authored with P. Abgrall, was published in 2009.